



Steady-state phases of the dissipative spin-1/2 XYZ model with frustrated interactionsXingli Li, Yan Li, and Jiasen Jin ^{*}*School of Physics, Dalian University of Technology, 116024 Dalian, China* (Received 21 July 2021; revised 17 September 2021; accepted 12 October 2021; published 20 October 2021)

We investigate the steady-state phases of the dissipative spin-1/2 J_1 - J_2 XYZ model on a two-dimensional square lattice. We show the next-nearest-neighbor interaction plays a crucial role in determining the steady-state properties. By means of the Gutzwiller mean-field (MF) factorization, we find the emergence of antiferromagnetic (AFM) steady-state phases. The existence of such AFM steady-state phases in thermodynamic limit is confirmed by cluster mean-field (CMF) analysis. Moreover, we find evidence of the limit cycle phase through the largest quantum Lyapunov exponent in small cluster and check the stability of the oscillation by calculating the averaged oscillation amplitude up to 4×4 CMF approximation.

DOI: [10.1103/PhysRevB.104.155130](https://doi.org/10.1103/PhysRevB.104.155130)**I. INTRODUCTION**

Quantum phase transition under equilibrium conditions has achieved a profound understanding in the past decades. The quantum phase transition is manifested by the continuous or abrupt changes of the ground state of a quantum many-body system when varying the external parameter. The spontaneous symmetry broken in the ground state is essentially driven by quantum fluctuations [1].

The phase transition in a quantum many-body system may also happen under the out-of-equilibrium condition. Actually, the inevitable interactions of a quantum system and its environment always drive the system, referred to as an open system, far from equilibrium. Because the thermal equilibrium is absent, the stationary property of the nonequilibrium system is determined by the asymptotical steady state of the nonunitary dynamics in the long-time limit. Usually, the dynamics of the open system in a Markovian (memoryless) environment is well described by the quantum master equation in Lindblad form $\dot{\hat{\rho}}(t) = \mathcal{L}\hat{\rho}(t)$, where \mathcal{L} is the so-called Liouvillian superoperator [2–4]. The properties of the steady state, as a result of the competition between the coherent evolution and the dissipative process, can be captured by the spectrum of \mathcal{L} [5]. Analogous to the equilibrium case, the steady-state symmetry ruled by the Lindblad master equation may also be spontaneously broken in the thermodynamic limit.

The steady-state phase diagram of the open quantum many-body system is predicted to be particularly rich [6–9]. It displays exotic phases that have spontaneously broken the symmetries possessed by the Liouvillian of the system [6,10–14]. Among the steady-state phases, the limit cycle (LC) phase, which spontaneously breaks the time translation invariance, has attracted significant attention [15–19]. It is considered to be a potential realization of time crystals in the nonequilibrium system [20–22]. Experimental investigations of nonequilibrium properties of open quantum many-body

systems have been realized in trapped ions [23], ultracold atomic gases in optical lattices [24–28], and arrays of coupled QED cavities [29–31].

Recently, it was explored that the frustration in a many-body system can induce fantastic nontrivial steady-state properties, such as the antiferromagnetism (AFM), spin-density wave, and chaotic dynamics [32–35]. The frustration refers to the fact that the competing interactions between neighboring sites cannot be satisfied simultaneously [36–38]. Generally, the presence of frustration is characterized by a large degeneracy in ground-state energy [39]. It is believed that the frustration tends to destroy conventional long-range orders. Basically, the frustration stems from either the geometry of the lattice or the competition among interactions in the system. We call the former the geometrical frustration and the latter the interaction frustration. One of the prototypes of the geometrically frustrated system is the two-dimensional Ising AFM on a triangular lattice. In this well-known model, the incompatible AFM interplay emerges once two of the spins are aligned oppositely to satisfy the AFM interaction and the third one cannot be antialigned to the other two spins simultaneously. The macroscopically degenerated ground state shows the fluidlike behavior [40,41]. The geometrical frustration has been realized experimentally [42–44]. Theoretically, it has been shown that in the geometrically frustrated spin-1/2 system on a triangular lattice, unconventional steady-state antiferromagnetism and spin-density wave emerge [32,33].

Regarding the competing-interaction frustrated system, the typical example is the J_1 - J_2 spin-1/2 Heisenberg model on square lattice in which both the nearest- (J_1) and the next-nearest- (J_2) neighboring (NNN) interactions are considered. The competition between the nearest-neighbor (NN) and NNN interactions dramatically modifies the Hamiltonian spectrum of the system with only NN interactions. The ratio J_1/J_2 determines the properties of the ground state of the system. In particular, for $J_1/J_2 < 1$, the ground state in the so-called Néel state, while in the opposite side $J_1/J_2 > 1$, is in the collinear striped antiferromagnetic (CAF) order [45,46]. In the intermediate region, the long-range order is suppressed

^{*}jsjin@dlut.edu.cn

by quantum fluctuations and the system is strongly frustrated. It is believed that the quantum spin liquid may exist in this region [47]. Inspired by the rich ground-state phase diagram induced by the competing NN and NNN interactions in the equilibrium case, we are going to investigate the steady-state properties of the open quantum many-body system with the J_1 - J_2 interactions. As a concrete example, we focus on a dissipative spin-1/2 XYZ model on two-dimensional square lattice. We consider both the NN and the NNN anisotropic Heisenberg couplings among the sites. In addition, the local dissipative processes on each site that drive the system out of equilibrium are considered taken into account. Our goal is to discover the novel steady-state phases that are brought by the NNN couplings. By employing a combination of state-of-the-art approaches, we shed light on the impact of NNN interactions in determining the steady state. As the NNN coupling varies, the system exhibits various steady-state phases. We mostly concentrate on the AFM phases. We also predict a LC phase in which the steady state is time periodic. In particular, the emergence of the LC phase is highlighted by the largest quantum Lyapunov exponent (LE) and averaged oscillation amplitude. The existence of LC phase is closely connected to the dissipative time crystals [14,21,22,48–50].

This paper is organized as follows. In Sec. II, we explain the dissipative spin-1/2 J_1 - J_2 XYZ model on the square lattice and the corresponding master equation that describes the evolution of the system. We present the possible steady-state phases that may appear in the system. In Sec. III, by employing the Gutzwiller single-site mean-field (MF) factorization, we solve the steady-state solutions to the single-site MF master equation. By performing linear stability analysis on the MF fixed points, we uncover the various steady-state phases. In Sec. IV, we include the short-range interaction in the discussion by performing the cluster mean-field (CMF) method. We confirm the existence of the CAF phase and show evidence of the LC phase through the largest LE and the average oscillation amplitude. We summarize in Sec. V.

II. MODEL

The model we consider here is a spin-1/2 quantum many-body model on square lattice whose Hamiltonian is given by (set $\hbar = 1$ hereinafter),

$$\hat{H} = \sum_{\alpha} J_{\alpha} \left[J_1 \sum_{\langle j,l \rangle} \hat{\sigma}_j^{\alpha} \hat{\sigma}_l^{\alpha} + J_2 \sum_{\langle\langle j,l \rangle\rangle} \hat{\sigma}_j^{\alpha} \hat{\sigma}_l^{\alpha} \right], \quad (1)$$

where $\hat{\sigma}_j^{\alpha}$ ($\alpha = x, y, z$) are the Pauli matrices for the j -th site; $\langle j, l \rangle$ and $\langle\langle j, l \rangle\rangle$ denote the sums of the spin-spin coupling run over the NN and NNN interactions, respectively; J_{α} are the coupling constants. For $J_2 = 0$, we recover the conventional XYZ model with NN couplings. The XYZ Hamiltonian is generic in spin systems and can be reduced to the isotropic Heisenberg Hamiltonian for $J_x = J_y = J_z$ and the Ising Hamiltonian for $J_x = J_y = 0$.

In order to drive the system out of equilibrium, we assume that each spin contacts with a Markovian environment which leads to a local dissipative process on each spin. In our specific model, the local environment tends to incoherently flip each spin down to the z direction. Thus the quantum master equa-

tion governing the evolution of the system's density-matrix $\hat{\rho}(t)$ is

$$\frac{d\hat{\rho}}{dt}(t) = \mathcal{L}[\hat{\rho}(t)] = -i[\hat{H}, \hat{\rho}(t)] + \sum_j \mathcal{D}_j[\hat{\rho}(t)], \quad (2)$$

where \mathcal{L} is the Liouvillian superoperator. The local dissipator \mathcal{D}_j on the j -th site takes the form of

$$\mathcal{D}_j[\hat{\rho}(t)] = \frac{\gamma}{2} [2\hat{\sigma}_j^- \hat{\rho}(t) \hat{\sigma}_j^+ - \hat{\sigma}_j^+ \hat{\sigma}_j^- \hat{\rho}(t) - \hat{\rho}(t) \hat{\sigma}_j^+ \hat{\sigma}_j^-], \quad (3)$$

where γ is the decay rate and the operators $\hat{\sigma}_j^{\pm} = (\hat{\sigma}_j^x \pm i\hat{\sigma}_j^y)/2$ represent the raising and lowering operators for the j -th spin. In the following, we will always work in units of γ . Additionally, for simplicity, we set $J_1/\gamma = 1$ and restrict the NNN coupling to be $J_2/\gamma \in (0, 1)$ in this work.

The Lindblad master equation Eq. (2) admits the \mathbb{Z}_2 symmetry associated to a π rotation of all the spins about the z axis ($\hat{\sigma}_j^x \rightarrow -\hat{\sigma}_j^x, \hat{\sigma}_j^y \rightarrow -\hat{\sigma}_j^y, \forall j$). In the thermodynamic limit, this \mathbb{Z}_2 symmetry may be spontaneously broken as the strengths of spin-spin interactions vary. In the symmetry-broken phases the magnetization on the x - y plane of each spin is nonzero and could be spatially modulated. Here we list the possible steady-state phases as the following:

(i) *Paramagnetic (PM) phase*. This is a trivial uniform state in which all the spins are pointing down along the z axis, $\langle \hat{\sigma}^x \rangle = \langle \hat{\sigma}^y \rangle = 0$ indicating that the system preserves the \mathbb{Z}_2 -symmetry. The notation $\langle \hat{\sigma}^{\alpha} \rangle = \text{tr}(\hat{\sigma}^{\alpha} \rho)$ ($\alpha = x, y, z$) means the expectation value of $\hat{\sigma}^{\alpha}$.

(ii) *Ferromagnetic (FM) phase*. The FM phase is a uniform ordered phase. Each spin has an identical nonzero steady-state magnetization on the xy plane, namely, $\langle \hat{\sigma}^x \rangle \neq 0, \langle \hat{\sigma}^y \rangle \neq 0$ as shown in Fig. 1(a), indicating that the \mathbb{Z}_2 -symmetry is broken.

(iii) *AFM phase*. The AFM phase is a nonuniform ordered phase. In the AFM phase, as shown in Fig. 1(b), the whole lattice is divided into two alternating sublattices. All the spins have nonzero steady-state magnetizations on the x - y plane. Moreover, the spin on one sublattice points to a different direction to the other. The steady-state magnetization is spatially modulated with a period of twice the lattice constant.

(iv) *CAF phase*. The CAF phase is another type of nonuniform ordered phase. In the CAF phase, the spins on the lattice are collinearly polarized. The steady-state magnetization is spatially modulated with a period of twice lattice constant in either the x or the y direction, as shown in Figs. 1(c) and 1(d).

The frustration in the J_1 - J_2 XYZ Hamiltonian

In this subsection, we check the existence of frustration in the studied Hamiltonian Eq. (1). We adopt the measure of frustration proposed in Refs. [51,52] which quantifies the incompatibility between the global and the local orders. A many-body Hamiltonian can be expressed as $\hat{H}_G = \sum_{\ell} \hat{h}_{\ell}$, where G stands for the global system and $\ell = \langle i, j \rangle$ or $\langle\langle i, j \rangle\rangle$ stands for the subsystem associated with local interactions \hat{h}_{ℓ} . The measure of frustration for \hat{h}_{ℓ} is defined as follows:

$$f_{\ell} = 1 - \text{tr}[\hat{\rho}_{\ell} \hat{\Pi}_{\ell}], \quad (4)$$

where $\hat{\rho}_{\ell} = \text{tr}_{\neq \ell} \hat{\rho}_G$ is the reduced local state obtained from the partial trace of the global ground state $\hat{\rho}_G$ of \hat{H}_G over the rest

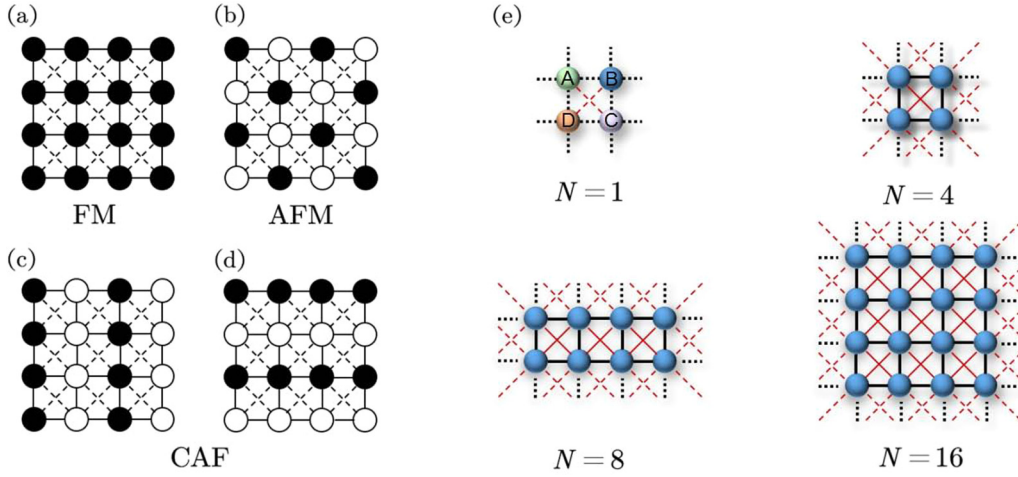


FIG. 1. (a)–(d) Illustration of partial \mathbb{Z}_2 -symmetry broken quantum phases in Heisenberg XYZ model; the black and white colors represent the different magnetization directions in x axis. (a) FM order; (b) AFM order; (c), (d) CAF order. (e) Schematic diagram of the Gutzwiller factorization of the full lattice. In the MF approximation ($N = 1$), the interactions between sites are all treated as an effective field (the dashed bonds), the lattice is divide into four sublattices (in different colors), marked by A, B, C , and D . For the CMF approximation with different sizes ($N \geq 4$), the interactions between the sites inside the cluster (the solid bonds) are treated exactly, the NN and NNN interactions outside of the cluster are treated as an effective field.

of the system, and $\hat{\Pi}_\ell$ is the projector onto the ground-state space of the local Hamiltonian \hat{h}_ℓ . The second term on the right-hand side of Eq. (4) quantifies the overlap between the reduced local state and the local ground state associated to \hat{h}_ℓ . Therefore the system is frustration-free if $f_\ell = 0, \forall \ell$. The total frustration of the global Hamiltonian is thus defined by averaging over all the local measures f_ℓ . This measure quantifies the frustrations due to the geometry of the system, the competing interactions, and the noncommutativity between different \hat{h}_ℓ s.

The effects of frustrations in the XYZ model with competing J_1 - J_2 interactions have been discussed in Ref. [53]. Here, in Fig. 2, we show the total frustration as a function of the strength of the NNN coupling of the XYZ model on a 4×4 lattice (open boundary condition). For the chosen parameters, one can see that the frustration is always present,

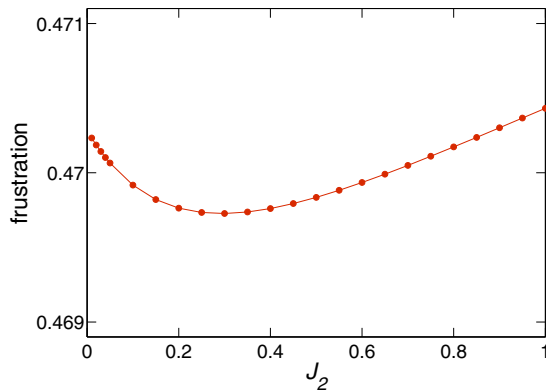


FIG. 2. The total frustration as a function of J_2 for the XYZ Hamiltonian on a 4×4 cluster (open boundary condition). The parameters are chosen as $\{J_x, J_y, J_z\} = \{-3.2, -1, 1\}$.

although the strength of NNN coupling affects the quantity of the frustration slightly. As will be seen in Sec. IV, the system exhibits various steady-state phases. Note that because the global ground state is twofold degenerate for the specific parameters, ρ_G is taken as the equiprobable statistical average of the two degenerate global ground states, namely, the maximally mixed global ground state [52].

III. MF APPROXIMATION

Due to the complexity of the full quantum master equation, we start with the single-site MF method basing on the Gutzwiller factorization. The density matrix for the whole lattice is factorized as $\hat{\rho} = \bigotimes_j \hat{\rho}_j$ with the reduced density-matrix $\rho_j = \text{tr}_{\neq j} \rho$ for each site. The reduced density matrices belong to the same sublattice and are assumed to be identical. Substituting the factorized density matrix into Eq. (2), we may obtain the single-site MF master equation for each sublattice in the following form,

$$\frac{d\hat{\rho}_j}{dt} = -i[\hat{H}_j^{\text{mf}}, \hat{\rho}_j] + \frac{\gamma}{2}[2\hat{\sigma}_j^- \hat{\rho}_j \hat{\sigma}_j^+ - \{\hat{\sigma}_j^+ \hat{\sigma}_j^-, \hat{\rho}_j\}], \quad (5)$$

where $j = A, B, C$, and D denotes the sublattice. The corresponding MF Hamiltonian for sublattice j is governed by

$$\hat{H}_j^{\text{mf}} = \sum_{\alpha=x,y,z} \sum_{k,l} J_\alpha \hat{\sigma}_j^\alpha (J_1 \langle \hat{\sigma}_k^\alpha \rangle + J_2 \langle \hat{\sigma}_l^\alpha \rangle), \quad (6)$$

where $\langle \hat{\sigma}_{j,l}^\alpha \rangle = \text{tr}(\hat{\sigma}_{j,l}^\alpha \hat{\rho}_{j,l})$, and the subscripts k and l denote the nearest and NNN of site j , respectively. By virtue of Eqs. (5) and (6), we obtain the following system of Bloch equations

for each sublattice as,

$$\begin{aligned} \frac{d\langle\hat{\sigma}_j^x\rangle}{dt} &= 2 \sum_l \sum_k J_y (J_1 \langle\hat{\sigma}_k^y\rangle + J_2 \langle\hat{\sigma}_l^y\rangle) \langle\hat{\sigma}_j^z\rangle - J_z (J_1 \langle\hat{\sigma}_k^z\rangle + J_2 \langle\hat{\sigma}_l^z\rangle) \langle\hat{\sigma}_j^y\rangle - \frac{\gamma}{2} \langle\hat{\sigma}_j^x\rangle, \\ \frac{d\langle\hat{\sigma}_j^y\rangle}{dt} &= 2 \sum_l \sum_k J_z (J_1 \langle\hat{\sigma}_k^z\rangle + J_2 \langle\hat{\sigma}_l^z\rangle) \langle\hat{\sigma}_j^x\rangle - J_x (J_1 \langle\hat{\sigma}_k^x\rangle + J_2 \langle\hat{\sigma}_l^x\rangle) \langle\hat{\sigma}_j^z\rangle - \frac{\gamma}{2} \langle\hat{\sigma}_j^y\rangle, \\ \frac{d\langle\hat{\sigma}_j^z\rangle}{dt} &= 2 \sum_l \sum_k J_x (J_1 \langle\hat{\sigma}_k^x\rangle + J_2 \langle\hat{\sigma}_l^x\rangle) \langle\hat{\sigma}_j^y\rangle - J_y (J_1 \langle\hat{\sigma}_k^y\rangle + J_2 \langle\hat{\sigma}_l^y\rangle) \langle\hat{\sigma}_j^x\rangle - \gamma (\langle\hat{\sigma}_j^z\rangle + 1), \end{aligned} \quad (7)$$

here again the sum over k, l is taken over the nearest and NNN of site j , respectively. The fixed points can be determined by setting Eq. (7) to be zero. Apparently, the state $\hat{\rho}_{j,\downarrow} = |\downarrow_j\rangle\langle\downarrow_j|$, with the spin pointing down to the z direction, is always a steady-state solution to Eq. (7). The joint state of the whole lattice is thus given by $\hat{\rho}_\downarrow = \bigotimes_j \hat{\rho}_{j,\downarrow}$ indicating that the system is in the PM phase. However, $\hat{\rho}_\downarrow$ is not always stable; the linear stability analysis on $\hat{\rho}_\downarrow$ can reveal the possibility of transitions from the PM to other phases.

The idea of linear stability analysis is to introduce local small fluctuations $\delta\rho_j$ to around the MF steady state by

$$\hat{\rho}_\downarrow \rightarrow \bigotimes_j (\hat{\rho}_{j,\downarrow} + \delta\rho_j) \quad (8)$$

and check how the perturbations evolve with time. We expand the perturbations in terms of plane waves

$$\delta\rho_j = \sum_{\mathbf{k}} e^{-i\mathbf{k}\cdot\mathbf{r}_j} \delta\rho_j^{\mathbf{k}}, \quad (9)$$

where \mathbf{k} is the wave vector. Thus the equation of motion for the perturbation $\delta\rho_j^{\mathbf{k}}$ is decoupled in the momentum space and reads,

$$\partial_t \delta\rho^{\mathbf{k}} = \mathcal{L}_{\mathbf{k}} \cdot \delta\rho^{\mathbf{k}}. \quad (10)$$

The superoperator $\mathcal{L}_{\mathbf{k}}$ has the following form,

$$\mathcal{L}_{\mathbf{k}} = \begin{pmatrix} -\gamma & 0 & 0 & 0 \\ 0 & P - \frac{\gamma}{2} & Q & 0 \\ 0 & -Q & -P - \frac{\gamma}{2} & 0 \\ \gamma & 0 & 0 & 0 \end{pmatrix}, \quad (11)$$

where the coefficients are given by $P = -i[(J_x + J_y)t_{\mathbf{k}} - 2\mathfrak{z}(1 + J_2)J_z]$, $Q = -i(J_x - J_y)t_{\mathbf{k}}$, $\mathfrak{z} = 4$ is the coordinate number, $t_{\mathbf{k}} = 2 \cos(k_x a) + 2 \cos(k_y a) + J_2 [e^{i(k_x + k_y)a} + e^{i(k_x - k_y)a} + e^{-i(k_x - k_y)a} + e^{-i(k_x + k_y)a}]$, and a is the lattice constant [10].

The steady state is dynamically stable when the real parts of all the eigenvalues of $\mathcal{L}_{\mathbf{k}}$ are negative; otherwise it is unstable to the perturbation of wave-vector $\mathbf{k} = (k_x, k_y)$. We define the most unstable eigenvalue λ_{\max} as the one with the largest positive real part; the wave-vector $\mathbf{k} = (k_x, k_y)$ associated to the most unstable eigenvalue can be used to distinguish distinct phases [33,54–57].

Additionally, we choose the initial states for each sublattice as $|\psi_A(0)\rangle = (|\uparrow\rangle + |\downarrow\rangle)/\sqrt{2}$, $|\psi_B(0)\rangle = (|\uparrow\rangle + e^{i\pi/2}|\downarrow\rangle)/\sqrt{2}$, $|\psi_C(0)\rangle = (|\uparrow\rangle + e^{i\pi}|\downarrow\rangle)/\sqrt{2}$ and $|\psi_D(0)\rangle = (|\uparrow\rangle + e^{i3\pi/2}|\downarrow\rangle)/\sqrt{2}$ to investigate the time evolution of the

system, although the steady states are independent of the initial states.

A. FM phase

We start with the phase transition from the PM to the FM phase. The critical point for the PM-FM phase transition can be obtained by solving Eq. (7); the explicit expression is given by

$$J_{x,y}^c = \frac{1}{16\mathfrak{z}^2(1 + J_2)^2(J_z - J_{y,x})} + J_z. \quad (12)$$

In Fig. 3, we show the time evolution of the magnetization $\langle\sigma^x(t)\rangle$ for $J_x = 1.01$ (PM phase) and 1.05 (FM phase) and $J_y = 0.9$. In the PM phase, the magnetizations of all the sites approach to zero after a sufficiently long time, regardless of the initial magnetization. While in the FM phase, after a transient oscillation, the state of each site first evolves a metastable

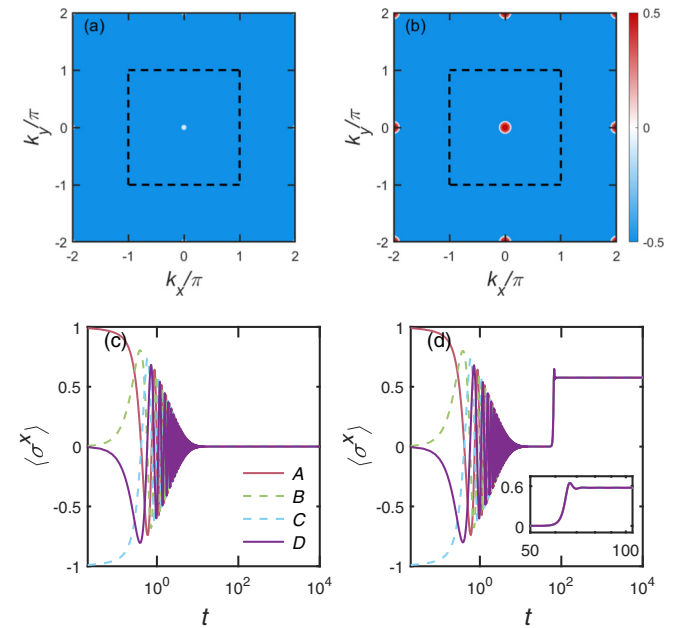


FIG. 3. (a), (b) The real part of the most unstable eigenvalue as a function of the wave-vectors k_x and k_y in momentum space. The dashed line indicates the first Brillouin zone. (c), (d) The MF steady-state magnetizations along the x direction for the sublattices. The parameters are chosen as $J_2 = 0.9$, $J_y = 0.9$, $J_z = 1$, and $J_x = 1.01$ for (a) and (c) and 1.05 for (b) and (d). The labels of sublattices are consistent with Fig. 1.

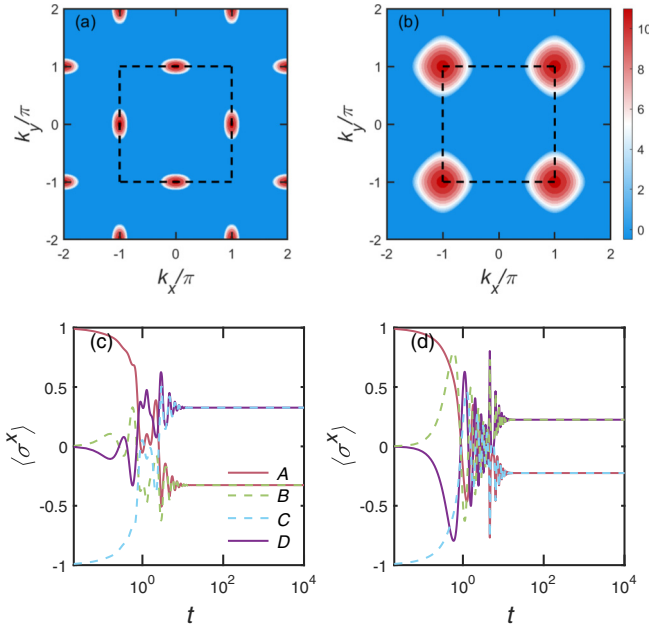


FIG. 4. (a), (b) The real part of the most unstable eigenvalue in momentum space. The dashed line indicates the first Brillouin zone. (c), (d) The MF steady-state magnetizations along the x direction for the sublattices. The parameters are chosen as $J_x = -2.5$, $J_y = 0.9$, $J_z = 1$, and $J_2 = 0.9$ for (a) and (c) and $J_2 = 0.1$ for (b) and (d). The labels of the sublattices are consistent with Fig. 1.

region with almost vanishing $\langle \sigma^x(t) \rangle$ and eventually ends up in the steady state with nonzero magnetization along the x direction. The appearance of the metastable state is because the chosen coupling parameter is close to the critical point.

In order to give the intuitive pictures for the PM and FM phases, we show the real parts of the most unstable eigenvalues in the momentum space in Fig. 3. For $J_x = 1.01$, the real part of λ_{\max} is always negative in the k_x - k_y plane indicating that $\hat{\rho}_\downarrow$ is stable against the perturbations. The maximum of the real part is about -0.0193 locating at the origin of the momentum space. As the coupling strength J_x increasing, the maximum of the real part increases and become positive in the FM phase. It is shown in Fig. 3 that the maximum is positive for $J_x = 1.05$ and the position of the maximum remains at the origin. In this case, the state $\hat{\rho}_\downarrow$ is unstable against uniform perturbations which offset each spin with a nonzero magnetization on the x - y plane. This indicates the appearance of the FM phase.

B. The PM-CAF transition

In this subsection, we discuss the phase transition from PM to AFM phases. Similarly to Eq. (12), one can obtain the expression for the critical point for PM-CAF transition as

$$J_{x,y}^c = -\frac{1}{16J_2[(1+J_2)J_z + J_2J_{y,x}]} - \frac{1+J_2}{J_2}J_z. \quad (13)$$

The real part of the most unstable eigenvalue in the momentum space in the CAF phase is shown in Fig. 4(a). The appearance of positive-valued maximum at $\mathbf{k} = (0, \pm\pi)$ and $(\pm\pi, 0)$ indicates that $\hat{\rho}_\downarrow$ is unstable against perturbations in

terms of plane wave along the x or y direction. Such perturbations give rise to a spatial modulation of the magnetizations along the x or y direction with the wavelength being twice the lattice constant. In Fig. 4(c), the time evolution of the magnetization $\langle \hat{\sigma}^x(t) \rangle$ for each sublattice is shown. One can see that the magnetizations $\langle \hat{\sigma}^x \rangle$ of the sublattices in the same column evolve to the same steady-state value for a sufficient long time indicating the CAF pattern.

Interestingly, we find that the CAF phase may become the AFM phase by varying the strength of NNN coupling J_2 . The real part of λ_{\max} in the momentum space in the AFM phase with $J_2 = 0.1$ is shown in Fig. 4(b). Compared to the case of CAF phase, in the AFM phase the positive maximum appears at $\mathbf{k} = (\pm\pi, \pm\pi)$ (the high-symmetry point M in the first Brillouin zone). This corresponds to the perturbation in both x and y directions. The steady-state magnetization is modulated in both directions with a period of two lattice sites; the whole lattice is actually divided into two sublattices. The steady-state pattern of the AFM state is also revealed by the time evolution of the magnetization $\langle \sigma^x \rangle$. From Fig. 4(d) one can see that magnetizations in the long-time limit exhibit $\langle \sigma_A^x \rangle = \langle \sigma_C^x \rangle \neq \langle \sigma_B^x \rangle = \langle \sigma_D^x \rangle$.

We recall that for $J_2 = 0$, the model reduces to the conventional XYZ model in which only the AFM phase exists [6]. In this sense, the CAF phase can be considered as a result of the presence of the NNN interaction and the competition to the NN interaction.

IV. CLUSTER MF METHOD

So far, we have neglected all the correlations in the discussion. In order to refine the MF results, we will take the short-range correlation into account in the analysis. To this aim, we apply the CMF technique to our model. In the CMF approximation, as schematically shown in Fig. 1(e), the whole lattice is divided into a series of clusters C which consist of a number of contiguous sites. All the clusters are assumed to be identical. The density matrix of the whole lattice is thus factorized as the product of the density matrix of each cluster,

$$\hat{\rho}_{\text{CMF}} = \bigotimes_C \hat{\rho}_C. \quad (14)$$

Substituting Eq. (14) into Eq. (2) and taking the partial trace of the global density matrix over all the clusters except for C , one can obtain the CMF master equation regarding cluster C as the following,

$$\frac{d\hat{\rho}_C}{dt} = -i[\hat{H}_{\text{CMF}}, \hat{\rho}_C] + \sum_{j \in C} \mathcal{D}_j[\hat{\rho}_C]. \quad (15)$$

In the expression above, the CMF Hamiltonian is given by

$$\hat{H}_{\text{CMF}} = \hat{H}_C + \hat{H}_{B(C)}, \quad (16)$$

where $\hat{H}_C = \sum_\alpha J_\alpha [J_1 \sum_{\langle(j,l) \in C} \hat{\sigma}_j^\alpha \hat{\sigma}_l^\alpha + J_2 \sum_{\langle\langle(j,l) \in C} \hat{\sigma}_j^\alpha \hat{\sigma}_l^\alpha]$ ($\alpha = x, y, z$, $\langle \cdot, \cdot \rangle$, and $\langle\langle \cdot, \cdot \rangle\rangle$ denote the NN and NNN sites) describes interactions between the sites inside the cluster C , while $\hat{H}_{B(C)} = \sum_\alpha J_\alpha [J_1 \sum_{\langle(j,l) \in C} \hat{\sigma}_j^\alpha \langle \hat{\sigma}_l^\alpha \rangle + J_2 \sum_{\langle\langle(j,l) \in C} \hat{\sigma}_j^\alpha \langle \hat{\sigma}_l^\alpha \rangle]$, where $j \in C$ and $l \in C'$ (C' is the cluster adjacent to C) describes the intercluster interactions. More details about the CMF approximation can be found in Ref. [57].

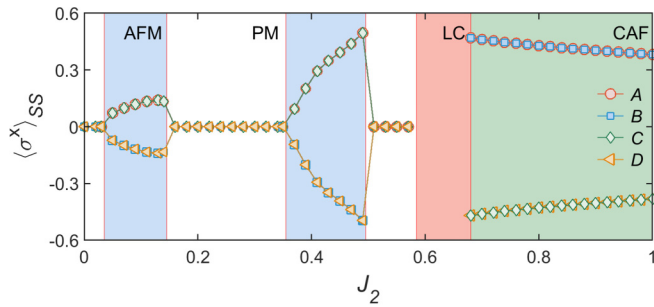


FIG. 5. The steady-state magnetizations along the x direction for a 2×2 cluster (each site indicated by various symbol) as a function of NNN coupling strength J_2 . In the LC region, the data are lacking since the system never reaches the asymptotical steady state in long-time limit. With J_2 increasing, the system exhibits the PM, AFM, LC, and CAF steady-state phases.

As shown in Eq. (16), the idea of CMF approximation is that the interactions between the sites inside a cluster are treated exactly, while the interactions between different clusters are treated at the mean-field level. In principle, as the size of the cluster is approaching to infinity and the correlations embedded in the lattice are gradually included in the analysis, we are able to obtain the property of the system in thermodynamic limit. The conventional MF approximation is considered to be a limit case for which all the correlations are neglected.

Here we will use a series of rectangular clusters of size $L = n_1 \times n_2$ in the CMF analysis. To be specific, for the clusters of size $L \leq 9$ we employ the standard fourth-order Runge-Kutta method to directly integrate the CMF master equation Eq. (15); for $L > 10$, we combine the CMF approximation with the quantum trajectory method [58–60] and the results are obtained by averaging over 500 trajectories [57].

We note that such rectangular clusters are convenient in revealing the FM or AFM nature of the steady states in our model because of their translation invariance along both x and y directions. Moreover, this choice simplifies the determination of the effective field in $\hat{H}_{B(C)}$. A series of clusters in other forms may also be used for CMF analysis, for instance, the clusters that can tile the square lattice [61]. The steady-state property of the system in thermodynamic limit is independent of the choice of clusters.

A. CAF phase

In Fig. 5, we show the CMF phase diagram as a function of J_2 with a cluster of size $L = 2 \times 2$; the other parameters are chosen as $\{J_x, J_y, J_z\} = \{-3.2, -1, 1\}$. One can see that as the strength of NNN coupling increases, the system exhibits various steady-state phases. For the limit cases of small and large J_2 , the steady-state phases are similar to those in the equilibrium system.

To corroborate the existence of the CAF phase, we investigate the steady-state magnetizations by systematically increasing the size of the clusters. In accordance with the definition of CAF phase, we choose the order parameter as $O_{CAF} = \sum_{j=1}^L \sum_{\langle\langle j,l \rangle\rangle} |\langle \sigma_j^x \rangle_{ss} - \langle \sigma_l^x \rangle_{ss}| / \ell$, where ℓ is the total number of NNN interactions. This order parameter shows the

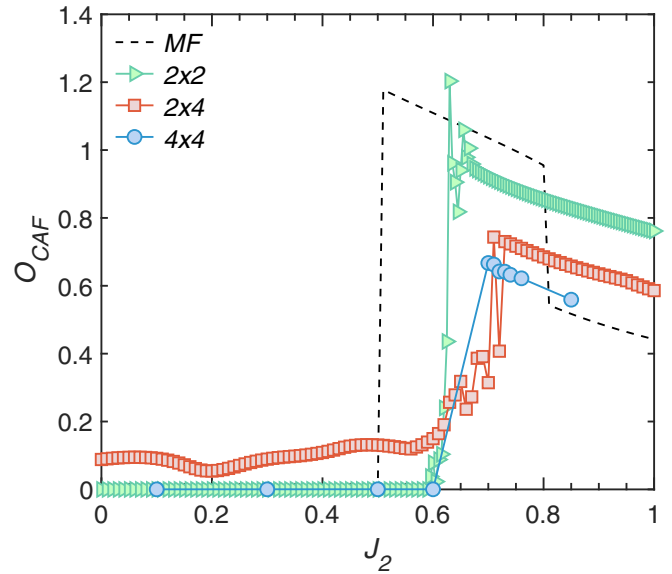


FIG. 6. The order-parameter O_{CAF} as a function of J_2 for various sizes of clusters. Other parameters are chosen as $\{J_x, J_y, J_z\} = \{-3.2, -1, 1\}$. The instable CMF data in $0.6 \leq J_2 \leq 0.7$ means the steady state of the system is.

steady-state magnetization difference between the j -th site and its NNN site. The nonzero value of O_{CAF} indicates the system is in the CAF phase.

In Fig. 6 we show the order-parameter O_{CAF} as a function of J_2 in the CMF approximation with different sizes of clusters. For the chosen anisotropic coupling case, both the single-site MF and the CMF results show the existence of the CAF phases at larger J_2 . As the size of the cluster increases, the CAF phase shrinks and remains in $0.7 \lesssim J_2 < 1$ up to a 4×4 cluster. One point that should be clarified is that the order-parameter O_{CAF} in the regions other than CAF phase is not exactly zero for the 2×4 cluster because of the geometrical anisotropy of the cluster.

B. Limit cycle

Interestingly, in the 2×2 CMF approximation, a LC region emerges for $0.59 \lesssim J_2 \lesssim 0.63$. In the LC region, the magnetization of each site oscillates periodically with time instead of reaching an asymptotic steady state in the long-time limit. The LCs are common in classical nonlinear dynamical systems and feature a stable closed trajectory in phase space. For the dissipative spin-1/2 XYZ model with only NN interaction, the LC is predicted by the single-site MF approximation [62,63]. On the contrary, here in our model with frustrated interactions, although the LC is missed by the single-site MF approximation, it is uncovered by the inclusion of short-range correlations in the CMF approximation.

In order to discriminate whether the time-dependent oscillation of the magnetization is a LC or chaos, we employ the so-called largest LE as proposed in Ref. [64].

Analogous to the classical definition, we use the quantum trajectories to simulate the evolution of the system. The largest LE is thus defined by the “distance” between the fiducial and the auxiliary trajectories. The “distance” may be obtained

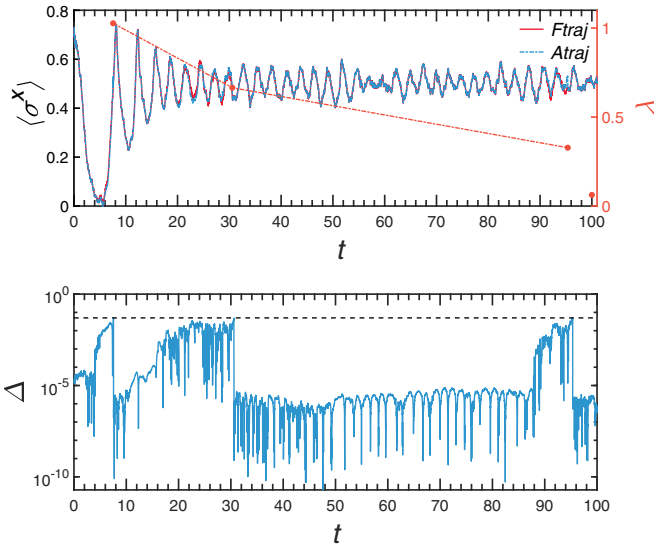


FIG. 7. The top panel shows the time-dependent magnetization $\langle \sigma^x \rangle$ of the fiducial trajectories (Ftraj) and auxiliary trajectories (Atraj). The red discrete dots represent the changing of the largest LE over time. The bottom panel shows changes of the difference of the observable Δ as a function time. The black dash line denotes the threshold $\Delta_{\max} = 0.05$ for resetting the auxiliary trajectory.

by direct calculation of the difference of some observables. In this work, we choose the observable to be the magnetization along the x direction $\bar{\sigma}^x(t)$, which can be obtained by

$$\bar{\sigma}^x(t) = \frac{1}{N} \sum_{j=1}^N \langle \psi_j(t) | \hat{\sigma}^x | \psi_j(t) \rangle. \quad (17)$$

The fiducial trajectory is initialized as a normalized quantum state vector ψ_f^{ini} , and the auxiliary one is also prepared as a normalized state with a perturbation on the fiducial initial state,

$$\psi_a^{\text{ini}} = \frac{\psi_f^{\text{ini}} + \delta\psi_p}{\|\psi_f^{\text{ini}} + \delta\psi_p\|}. \quad (18)$$

Here ψ_p is a random perturbative state and $\delta \ll 1$. The difference of observables $\Delta(t) = |\bar{\sigma}_f^x(t) - \bar{\sigma}_a^x(t)|$ is time dependent. The initial value can be calculated by $\Delta_0 = |\bar{\sigma}_f^x(0) - \bar{\sigma}_a^x(0)|$. If the difference exceeds threshold $\Delta(t_k) > \Delta_{\max}$ at time t_k , the growth factor of the largest LE $d_k = \Delta(t_k)/\Delta_0$ is summed and the auxiliary state vectors have to be renormalized close to the fiducial trajectories. The difference of observables is reset to the initial value. The largest LE can be estimated as

$$\lambda = \lim_{t \rightarrow \infty} \frac{1}{t} \sum_k \ln d_k. \quad (19)$$

Here we discuss the cluster of size $L = 2 \times 2$. In the simulation, the number of trajectories is $M = 300$ and the threshold is $\Delta_{\max} = 0.05$. The numerical result is shown in Fig. 7. In the top panel, the left y axis corresponds to the time evolution of on-site magnetization for fiducial and auxiliary trajectories, $\bar{\sigma}_f^x(t)$ and $\bar{\sigma}_a^x(t)$, respectively. Although the amplitude of the oscillation fluctuates due to the probabilistic nature

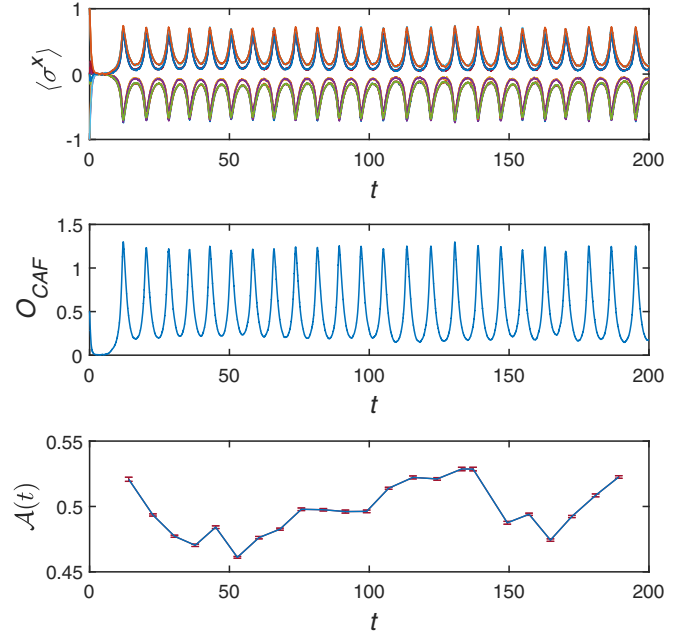


FIG. 8. The top panel presents the time-dependent magnetization $\langle \sigma_j^x \rangle$ for a 4×4 cluster. The middle panel shows the time-dependent order-parameter O_{CAF} , the time-dependent average amplitude is shown in the bottom panel, the error bars denote the variances of the average amplitude, and the parameters are chosen as $J_x = -3.2$, $J_y = -1$, $J_z = 1$, and $J_2 = 0.63$.

of the quantum trajectory method, the significant oscillating behavior can be observed. The right y axis is related to the change of the largest LE with evolution time. The largest LE is updated three times in the time interval of $t \in [0, 100]$, corresponding to the time at which the difference exceeds the threshold. We have extended the simulation to $t = 500$; the largest LE descends from $\{\lambda, t\} = \{1.0269, 7.5645\}$ to $\{\lambda, t\} = \{0.0625, 500\}$. The largest LE at $t = 500$ is shown by the most-right orange symbol.

The bottom panel is the time evolution of the difference of observables $\Delta(t)$. It can be seen that there are three discontinuous jumps at $t \approx 8, 30$, and 96 . The jumps mark the events that the difference of observables exceeds the threshold. The difference at $t = 500$ is $\Delta < 3 \times 10^{-10}$ (not shown), which is small enough to indicate that the largest LE will continue to descend in the long-time limit. We can conclude that the $\Delta(t)$ will eventually reach zero and the oscillation is stable.

In the upper panel of Fig. 8, we show the time evolution of the magnetization for each sublattice in the LC region with the 4×4 CMF approximation. The time dependence of the CAF order parameter is shown in the middle panel as well. One can see that the magnetization is time dependent and showing a CAF pattern. As reported in Refs. [62,63], the LC is absent in the case of $J_2 = 0$; the coexistence of the CAF ordering and oscillating magnetization is a combination of the effects of the interaction frustration and nonequilibrium nature of the system. To check the stability of the oscillation, we define $\mathcal{A}(t) = \sum_{j=1}^L \mathcal{A}[\langle \hat{\sigma}_j^x \rangle] / L$, where $\mathcal{A}[\langle \hat{\sigma}_j^x \rangle]$ measures the difference between the local maximum and minimum values. The averaged amplitude $\mathcal{A}(t)$ is shown in the bottom

panel of Fig. 8. The error bars are the variances of the average oscillation amplitude. In each oscillation period, the peaks or the valleys of the time-dependent magnetization of each site do not always accurately locate at the same time. After determining the local maximum t_{\max}^{loc} or minimum time point t_{\min}^{loc} for each magnetization, we average each magnetization over a small time window Δt to obtain the amplitude, e.g., $\Delta t = t_{\max}^{\text{loc}} \pm \delta t$, $\delta t = 0.4$. Without considering the fluctuations $\mathcal{A}(t)$ caused by the probabilistic nature of the quantum trajectory method, the value of $\mathcal{A}(t)$ stays in the range $0.45 \leq \mathcal{A}(t) \leq 0.55$ indicating that the oscillation is stable.

V. SUMMARY

In summary, we have investigated the steady-state phases of the dissipative spin-1/2 XYZ model with J_1 - J_2 couplings. Compared with the previous studies on the same model but with only NN couplings (J_1), the presence of the interaction frustration induced by the NNN coupling (J_2) indeed enriches the steady-state phases. In order to study the dynamics of the system, we perform the MF approximation, based on the Gutzwiller factorization, to decouple the master equation that governs the dynamics of the whole lattice. We check the linear stability of the fixed points to the system of single-site MF Bloch equations. The results from the single-site MF approximation reveal the emergence of the various AFM phases, including the AFM and CAF phases. The critical point of the PM-CAF phase transition is presented.

The formalism of the linear stability analysis reminds us of the well-known spin-wave theory in determining the low-energy excitation of the magnetically ordered system. In the spin-wave theory, the spins of the considered system are assumed to be aligned in the same direction. The wave-like low-energy excitation is created by the spin operator in the reciprocal lattice $\hat{S}_{\mathbf{k}} = \sum_j e^{i\mathbf{k}\cdot\mathbf{r}_j} \hat{S}_j$. The thermodynamics properties as well as the dynamics of the considered sys-

tem can thus be investigated by the diagonalization of the Hamiltonian in the momentum space. Recently, the spin-wave approximation has been used in studying the effect of the external magnetic field in the quantum spin system which is described by the Karplus-Schwinger master equation [65]. The application of spin-wave approximation to open quantum systems would be an interesting topic.

The existence of the AFM phases in the thermodynamic limit is confirmed by a series of CMF analysis. The short-range correlations are gradually included as the size of clusters increases. The CAF order remains nonzero up to the 4×4 CMF approximation. Moreover, we find evidence of the LC phase, in which the system is in a time-periodic oscillating state in the long-time limit, in the CMF approximation. The fact that the LC phase is absent in single-site MF approximation but appears in the CMF approximation is the unique feature in the interaction frustrated system. The investigations on the largest quantum LE and the averaged oscillation amplitude support the existence of the LC phase up to the 4×4 CMF approximation.

Finally, we note that the properties of the steady-state phases investigated in this paper, especially the stability of the LC phase, are limited by the cluster size; analysis on the larger size cluster is still required. On this perspective, the combination of the CMF approach with other available techniques is promising to achieve this purpose, such as machine learning techniques [66–70] and corner-space renormalization [71,72]. A comprehensive panorama of the simulation methods for open quantum many-body systems can be found in Ref. [73]. In addition, our theoretical predictions may be experimentally investigated in following different platforms [74–76].

ACKNOWLEDGMENT

This work is supported by National Natural Science Foundation of China via Grant No. 11975064.

-
- [1] S. Sachdev, *Quantum Phase Transitions* (Cambridge University Press, Cambridge, 2000).
 - [2] H.-P. Breuer and F. Petruccione, *The Theory of Open Quantum Systems* (Oxford University Press, New York, 2002).
 - [3] G. Lindblad, On the generators of quantum dynamical semigroups, *Commun. Math. Phys.* **48**, 119 (1976).
 - [4] V. Gorini, A. Kossakowski, and E. C. G. Sudarsahan, Completely positive dynamical semigroups of N-level systems, *J. Math. Phys.* **17**, 821 (1976).
 - [5] F. Minganti, A. Biella, N. Bartolo, and C. Ciuti, Spectral theory of Liouvillians for dissipative phase transitions, *Phys. Rev. A* **98**, 042118 (2018).
 - [6] T. E. Lee, S. Gopalakrishnan, and M. D. Lukin, Unconventional Magnetism Via Optical Pumping of Interacting Spin Systems, *Phys. Rev. Lett.* **110**, 257204 (2013).
 - [7] V. Savona, Spontaneous symmetry breaking in a quadratically driven nonlinear photonic lattice, *Phys. Rev. A* **96**, 033826 (2017).
 - [8] J. Jin, A. Biella, O. Viyuela, C. Ciuti, R. Fazio, and D. Rossini, Phase diagram of the dissipative quantum Ising model on a square lattice, *Phys. Rev. B* **98**, 241108(R) (2018).
 - [9] D. Huybrechts, F. Minganti, F. Nori, M. Wouters, N. Shammah, Mean-field validity in a dissipative critical system: Liouvillian gap, PT-symmetric antigap, and permutational symmetry in the XYZ model, *Phys. Rev. B* **101**, 214302 (2020).
 - [10] T. E. Lee, H. Häffner, and M. C. Cross, Antiferromagnetic phase transition in a nonequilibrium lattice of Rydberg atoms, *Phys. Rev. A* **84**, 031402(R) (2011).
 - [11] J. Jin, D. Rossini, R. Fazio, M. Leib, and M. J. Hartmann, Photon Solid Phases in Driven Arrays of Nonlinearly Coupled Cavities, *Phys. Rev. Lett.* **110**, 163605 (2013).
 - [12] H. Weimer, Variational Principle for Steady States of Dissipative Quantum Many-Body Systems, *Phys. Rev. Lett.* **114**, 040402 (2015).
 - [13] V. R. Overbeck, M. F. Maghrebi, A. V. Gorshkov, and H. Weimer, Multicritical behavior in dissipative Ising models, *Phys. Rev. A* **95**, 042133 (2017).
 - [14] H. Landa, M. Schiró, and G. Misguich, Correlation-induced steady states and limit cycles in driven dissipative quantum systems, *Phys. Rev. B* **102**, 064301 (2020).
 - [15] M. Ludwig and F. Marquardt, Quantum Many-Body Dynamics in Optomechanical Arrays, *Phys. Rev. Lett.* **111**, 073603 (2013).

- [16] W. Li, C. Li, and H. Song, Quantum synchronization in an optomechanical system based on Lyapunov control, *Phys. Rev. E* **93**, 062221 (2016).
- [17] M. Xu, D. A. Tieri, E. C. Fine, J. K. Thompson, and M. J. Holland, Synchronization of Two Ensembles of Atoms, *Phys. Rev. Lett.* **113**, 154101 (2014).
- [18] T. E. Lee, C.-K. Chan, and S. Wang, Entanglement tongue and quantum synchronization of disordered oscillators, *Phys. Rev. E* **89**, 022913 (2014).
- [19] C. Davis-Tilley, C. K. Teoh, and A. D. Armour, Dynamics of many-body quantum synchronisation, *New J. Phys.* **20**, 113002 (2018).
- [20] Z. Gong, R. Hamazaki, and M. Ueda, Discrete Time-Crystalline Order in Cavity and Circuit QED System, *Phys. Rev. Lett.* **120**, 040404 (2018).
- [21] F. Iemini, A. Russomanno, J. Keeling, M. Schiró, M. Dalmonte, and R. Fazio, Boundary Time Crystals, *Phys. Rev. Lett.* **121**, 035301 (2018).
- [22] K. Tucker, B. Zhu, R. J. Lewis-Swan, J. Marino, F. Jimenez, J. G. Restrepo, and A. M. Rey, Shattered time: Can a dissipative time crystal survive many-body correlations? *New J. Phys.* **20**, 123003 (2018).
- [23] M. Müller, S. Diehl, G. Pupillo, and P. Zoller, Engineered open systems and quantum simulations with atoms and ions, *Adv. At. Mol. Opt. Phys.* **61**, 1 (2012).
- [24] M. Greiner, O. Mandel, T. Esslinger, T. W. Hänsch, and I. Bloch, Quantum phase transition from a superfluid to a Mott insulator in a gas of ultracold atoms, *Nature (London)* **415**, 39 (2002).
- [25] I. Bloch, J. Dalibard, and W. Zwerger, Many-body physics with ultracold gases, *Rev. Mod. Phys.* **80**, 885 (2008).
- [26] K. Baumann, R. Mottl, F. Brennecke, and T. Esslinger, Exploring Symmetry Breaking at the Dicke Quantum Phase Transition, *Phys. Rev. Lett.* **107**, 140402 (2011).
- [27] K. Baumann, C. Guerlin, F. Brennecke, and T. Esslinger, Dicke quantum phase transition with a superfluid gas in an optical cavity, *Nature (London)* **464**, 1301 (2010).
- [28] D. Bluvstein, A. Omran, H. Levine, A. Keesling, G. Semeghini, S. Ebadi, T. T. Wang, A. A. Michailidis, N. Maskara, W. W. Ho, S. Choi, M. Serbyn, M. Greiner, V. Vuletic, M. D. Lukin, Controlling quantum many-body dynamics in driven Rydberg atom arrays, *Science* **371**, 1355 (2021).
- [29] A. A. Houck, H. E. Türeci and J. Koch, On-chip quantum simulation with superconducting circuits, *Nat. Phys.* **8**, 292 (2012).
- [30] M. Fitzpatrick, N. M. Sundaresan, A. C. Y. Li, J. Koch, and A. A. Houck, Observation of a Dissipative Phase Transition in a One-Dimensional Circuit QED Lattice, *Phys. Rev. X* **7**, 011016 (2017).
- [31] M. C. Collodo, A. Potočnik, S. Gasparinetti, J.-C. Besse, M. Pechal, M. Sameti, M. J. Hartmann, A. Wallraff, and C. Eichler, Observation of the Crossover from Photon Ordering to Delocalization in Tunably Coupled Resonators, *Phys. Rev. Lett.* **122**, 183601 (2019).
- [32] J. Qian, L. Zhou, and W. Zhang, Quantum phases of strongly interacting Rydberg atoms in triangular lattices, *Phys. Rev. A* **87**, 063421 (2013).
- [33] X. Li and J. Jin, Nonuniform phases in the geometrically frustrated dissipative XYZ model, *Phys. Rev. B* **103**, 035127 (2021).
- [34] J. Qiao, W. Chang, X. Li and J. Jin, Numerical linked-cluster expansion for the dissipative XYZ model on a triangular lattice, *J. Phys. Commun.* **4**, 015020 (2020).
- [35] Z. Li, A. Soret, and C. Ciuti, Dissipation-induced antiferromagnetic-like frustration in coupled photonic resonators, *Phys. Rev. A* **103**, 022616 (2021).
- [36] F. Figueirido, A. Karlhede, S. Kivelson, S. Sondhi, M. Rocek, and D. S. Rokhsar, Exact diagonalization of finite frustrated spin-1/2 Heisenberg models, *Phys. Rev. B* **41**, 4619 (1990).
- [37] D. Yamamoto, G. Marmorini, and I. Danshita, Quantum Phase Diagram of the Triangular-Lattice XXZ Model in a Magnetic Field, *Phys. Rev. Lett.* **112**, 127203 (2014).
- [38] S. Yan, D. A. Huse and S. R. White, Spin-liquid ground state of the $S = 1/2$ Kagome Heisenberg antiferromagnet, *Science* **332**, 1173 (2011).
- [39] G. H. Wannier, Antiferromagnetism. The triangular Ising net, *Phys. Rev.* **79**, 357 (1950).
- [40] J. Wen, S.-L. Yu, S. Li, W. Yu, and J.-X. Li, Experimental identification of quantum spin liquids, *npj Quantum Mater.* **4**, 12 (2019).
- [41] Y. Zhou, K. Kanoda, and T.-K. Ng, Quantum spin liquid states, *Rev. Mod. Phys.* **89**, 025003 (2017).
- [42] K. Kim, M.-S. Chang, S. Korenblit, R. Islam, E. E. Edwards, J. K. Freericks, G.-D. Lin, L.-M. Duan, and C. Monroe, Quantum simulation of frustrated Ising spins with trapped ions, *Nature (London)* **465**, 590 (2010).
- [43] A. Eckardt, P. Hauke, P. Soltan-Panahi, C. Becker, K. Sengstock, and M. Lewenstein, Frustrated quantum antiferromagnetism with ultracold bosons in a triangular lattice, *Europhys. Lett.* **89**, 10010 (2010).
- [44] C. Becker, P. Soltan-Panahi, J. Kronjäger, S. Dörscher, K. Bongs, and K. Sengstock, Ultracold quantum gases in triangular optical lattices, *New J. Phys.* **12**, 065025 (2010).
- [45] O. Götze, S. E. Krüger, F. Fleck, J. Schulenburg, and J. Richter, Ground-state phase diagram of the spin-1/2 square-lattice J_1 - J_2 model with plaquette structure, *Phys. Rev. B* **85**, 224424 (2012).
- [46] Z.-Q. Yu and L. Yin, Collinear antiferromagnetic state in a two-dimensional Hubbard model at half filling, *Phys. Rev. B* **81**, 195122 (2010).
- [47] W.-Y. Liu, S.-S. Gong, Y.-B. Li, D. Poilblanc, W.-Q. Chen, and Z.-C. Gu, Gapless quantum spin liquid and global phase diagram of the spin-1/2 J_1 - J_2 square antiferromagnetic Heisenberg model, *arXiv:2009.01821* (2020).
- [48] C.-h. Fan, D. Rossini, H.-X. Zhang, J.-H. Wu, M. Artoni, and G. C. La Rocca, Discrete time crystal in a finite chain of Rydberg atoms without disorder, *Phys. Rev. A* **101**, 013417 (2020).
- [49] K. Seibold, R. Rota, and V. Savona, Dissipative time crystal in an asymmetric nonlinear photonic dimer, *Phys. Rev. A* **101**, 033839 (2020).
- [50] L. F. dos Prazeres, L. da Silva Souza, and F. Iemini, Boundary time crystals in collective d-level systems, *Phys. Rev. B* **103**, 184308 (2021).
- [51] S. M. Giampaolo, G. Gualdi, A. Monras, and F. Illuminati, Characterizing and Quantifying Frustration in Quantum Many-body Systems, *Phys. Rev. Lett.* **107**, 260602 (2011).
- [52] U. Marzolino, S. M. Giampaolo, and F. Illuminati, Frustration, entanglement, and correlations in quantum many-body systems, *Phys. Rev. A* **88**, 020301(R) (2013).

- [53] S. M. Giampaolo, B. C. Hiesmayr, and F. Illuminati, Global-to-local incompatibility, monogamy of entanglement, and ground-state dimerization: Theory and observability of quantum frustration in systems with competing interactions, *Phys. Rev. B* **92**, 144406 (2015).
- [54] M. C. Cross and P. C. Hohenberg, Pattern formation outside of equilibrium, *Rev. Mod. Phys.* **65**, 851 (1993).
- [55] A. Le Boité, G. Orso, and C. Ciuti, Steady-State Phases and Tunneling-Induced Instabilities in the Driven Dissipative Bose-Hubbard Model, *Phys. Rev. Lett.* **110**, 233601 (2013).
- [56] A. Le Boité, G. Orso, and C. Ciuti, Bose-Hubbard model: Relation between driven-dissipative steady states and equilibrium quantum phases, *Phys. Rev. A* **90**, 063821 (2014).
- [57] J. Jin, A. Biella, O. Viyuela, L. Mazza, J. Keeling, R. Fazio, and D. Rossini, Cluster Mean-Field Approach to the Steady-State Phase Diagram of Dissipative Spin Systems, *Phys. Rev. X* **6**, 031011 (2016).
- [58] K. Mølmer, Y. Castin, and J. Dalibard, Monte Carlo wavefunction method in quantum optics, *J. Opt. Soc. Am. B* **10**, 524 (1993).
- [59] J. Dalibard, Y. Castin, and K. Mølmer, Wave-Function Approach to Dissipative Processes in Quantum Optics, *Phys. Rev. Lett.* **68**, 580 (1992).
- [60] M. B. Plenio and P. L. Knight, The quantum-jump approach to dissipative dynamics in quantum optics, *Rev. Mod. Phys.* **70**, 101 (1998).
- [61] E. Dagotto, Correlated electrons in high-temperature superconductors, *Rev. Mod. Phys.* **66**, 763 (1994).
- [62] C.-K. Chan, T. E. Lee and S. Gopalakrishnan, Limit-cycle phase in driven-dissipative spin systems, *Phys. Rev. A* **91**, 051601(R) (2015).
- [63] E. T. Owen, J. Jin, D. Rossini, R. Fazio, M. J. Hartmann, Quantum correlations and limit cycles in the driven-dissipative Heisenberg lattice, *New J. Phys.* **20**, 045004 (2018).
- [64] I. I. Yusipov, O. S. Vershinina, S. Denisov, S. P. Kuznetsov, and M. V. Ivanchenko, Quantum Lyapunov exponents beyond continuous measurements, *Chaos* **29**, 063130 (2019).
- [65] A. A. Zvyagin, Modulation of the longitudinal pumping in quantum spin systems, *Phys. Rev. B* **101**, 174408 (2020).
- [66] M. J. Hartmann and G. Carleo, Neural-Network Approach to Dissipative Quantum Many-Body Dynamics, *Phys. Rev. Lett.* **122**, 250502 (2019).
- [67] A. Nagy and V. Savona, Variational Quantum Monte Carlo Method with a Neural-Network Ansatz for Open Quantum Systems, *Phys. Rev. Lett.* **122**, 250501 (2019).
- [68] F. Vicentini, A. Biella, N. Regnault, and C. Ciuti, Variational Neural-Network Ansatz for Steady States in Open Quantum Systems, *Phys. Rev. Lett.* **122**, 250503 (2019).
- [69] N. Yoshioka and R. Hamazaki, Constructing neural stationary states for open quantum many-body systems, *Phys. Rev. B* **99**, 214306 (2019).
- [70] D. Yuan, H. Wang, Z. Wang, and D.-L. Deng, Solving the Liouvillian Gap with Artificial Neural Networks, *Phys. Rev. Lett.* **126**, 160401 (2021).
- [71] S. Finazzi, A. Le Boité, F. Storme, A. Baksic, and C. Ciuti, Corner-Space Renormalization Method for Driven-Dissipative Two-Dimensional Correlated Systems, *Phys. Rev. Lett.* **115**, 080604 (2015).
- [72] R. Rota, F. Minganti, C. Ciuti, and V. Savona, Quantum Critical Regime in a Quadratically Driven Nonlinear Photonic Lattice, *Phys. Rev. Lett.* **122**, 110405 (2019).
- [73] H. Weimer, A. Kshetrimayum, and R. Orús, Simulation methods for open quantum many-body systems, *Rev. Mod. Phys.* **93**, 015008 (2021).
- [74] D. Porras and J. I. Cirac, Effective Quantum Spin Systems with Trapped Ions, *Phys. Rev. Lett.* **92**, 207901 (2004).
- [75] R. Melzi, S. Aldrovandi, F. Tedoldi, P. Carretta, P. Millet, and F. Mila, Magnetic and thermodynamic properties of $\text{Li}_2\text{VOSiO}_4$: A two-dimensional $S = 1/2$ frustrated antiferromagnet on a square lattice, *Phys. Rev. B* **64**, 024409 (2001).
- [76] H. Ishikawa, N. Nakamura, M. Yoshida, M. Takigawa, P. Babkevich, N. Qureshi, H. M. Rønnow, T. Yajima, and Z. Hiroi, J_1 - J_2 square-lattice Heisenberg antiferromagnets with $4d^1$ spins: AMoOPO_4Cl ($A = \text{K, Rb}$), *Phys. Rev. B* **95**, 064408 (2017).